Biohybrid photoprotein-semiconductor cells with deep-lying redox shuttles achieve a 0.7 V photovoltage

Varun Kumar Singh [a†], Sai Kishore Ravi [a†], Ho Jian Wei[b], Johnson Kai Chi Wong[b], Michael R. Jones[c] and Swee Ching Tan[*a]

[a]*Department of Materials Science and Engineering, National University of Singapore, 9 Engineering Drive 1, Singapore 117574*

[b]*Solar Energy Research Institute of Singapore (SERIS), National University of Singapore (NUS), 7 Engineering Drive 1, Singapore 117574*

[c]*School of Biochemistry, Biomedical Sciences Building, University of Bristol, University Walk, Bristol, BS8 1TD, UK*

[*]Corresponding author: msetansc@nus.edu.sg

[†]The two authors contributed equally to the work.

Abstract

Photosynthetic proteins transduce sunlight into biologically-useful forms of energy through a photochemical charge separation that has a close to 100% quantum efficiency, and there is increasing interest in their use as sustainable materials in biohybrid devices for solar energy harvesting. This work explores a new strategy for boosting the open-circuit voltage of photoelectrochemical cells based on a bacterial photosynthetic pigment-protein by employing highly oxidising redox electrolytes in conjunction with an n-type silicon anode. Illumination generates electron-hole pairs in both the protein and the silicon electrode, the two being connected by the electrolyte which transfers electrons from the reducing terminal of the protein to photogenerated holes in the silicon valence band. A high open circuit voltage of 0.6 V was achieved with the most oxidizing electrolyte TEMPO (2,2,6,6-tetramethyl-1-piperidinyloxy), and this was further improved to 0.7 V on surface modification of the silicon electrode to increase its surface area and reduce reflection of incident light. The photovoltages produced by these biohybrid protein/silicon cells are comparable to those typical of silicon heterojunction and dye-sensitized solar cells.

Key Words: Solar Energy Harvesting; Photosynthetic Proteins; Open Circuit Voltage Enhancement; Redox electrolytes; Photo-bioelectrochemical cells

Introduction

Against a background of concerns over how future projections of energy demand can be addressed through environmentally benign and sustainable technologies, there is increasing interest in the development of a diversity of novel approaches to solar energy conversion. One option that exploits naturally available materials is to use light harvesting and photovoltaic pigment-proteins from photosynthetic organisms as components in biohybrid photoelectrochemical cells[1, 2, 3, 4, 5, 6, 7, 8, 9]. Most of the progress in this area has been made with the Photosystem I complex from oxygenic phototrophs [7, 10, 11, 12, 13, 14, 15] and the reaction centre (RC) from the anoxygenic photosynthetic bacterium *Rhodobacter* (*Rba.*) *sphaeroides*[9, 16, 17, 18, 19, 20, 21, 22, 23, 24, 25, 26, 27]. In addition to exploration of their photovoltaic capacities, these proteins have been evaluated for applications in molecular electronics[4], photosensing[28], biosensing[29, 30] and the synthesis of molecular fuels[31]. Part of the attraction of using natural photovoltaic materials for solar energy conversion is their high quantum yield (charges separated per photon absorbed), which stems from efficient light harvesting and a multi-step mechanism for charge separation that is unidirectional and minimally affected by charge recombination[32, 33].

The *Rba. sphaeroides* RC, and the RC-LH1 macromolecular complex it forms with the LH1 light harvesting protein, are tractable and well characterised systems that have been used extensively to explore the molecular basis of solar energy conversion during natural photosynthesis[34, 35, 36, 37, 38]. The light harvesting bacteriochlorophyll (BChl) and carotenoid pigments of the LH1 protein absorb sunlight across the visible and near-infrared spectral regions and focus excited state energy on an electron transfer chain in the central RC domain (Figure 1a). Arrival of excitation energy at a pair of BChls in the RC protein (denoted P) triggers a meta-stable separation of electrical charge through a four-step transfer of an electron across the RC to a dissociable ubiquinone (Q_B), forming the radical pair $P^+Q_B^-$ [34, 35, 36, 39]. This charge separation takes place in a few hundred microseconds and has a lifetime of over a second, with a difference in potential of around 0.5 V between the P/P^+ and Q_B/Q_B^- redox couples (Figure 1b). As the lowest energy singlet excited state of the P BChls (denoted P*) has an energy of 1.45 eV relative to the ground state, this means that around one third of the energy required to trigger charge separation is conserved in the final radical pair. The remainder is sacrificed to ensure that each step of charge separation is effectively irreversible and that losses through charge recombination are minimised.

In the main, published studies of solar energy conversion by RCs and RC-LH1 complexes in biohybrid photoelectrochemical cells have focussed on the mechanism of photocurrent generation and the control of protein/electrode interactions, with relatively little attention given to the open circuit voltage (V_{OC}) or its optimisation. A handful of studies have reported values of V_{OC} that range between 7 and 140 mV [17, 26, 27, 40, 41, 42]. In typical device architectures the V_{OC} of a cell based on a RC or RC-LH1 protein is expected to be limited by the potential gap between the molecular species receiving electrons from the cathode and the species donating electrons to the anode. These may be components of the protein, usually the P^+ and Q_B^- redox centres at either end of the internal charge separation chain, or one or more electrolytes that provide the electrical connection to one or both electrodes. In the schematic in Figure 1b, which is based on previous works[20, 21, 25, 43], where the P^+ species in RC-LH1 complexes adjacent to an FTO-glass anode receives electrons directly, and a mediator moves charge from the "negative terminal" of the RC-LH1 complex to the counter electrode. The V_{OC} of such a cell is expected to be dependent on the potential gap between the P/P^+ couple that interfaces with the cathode and the mediator that interfaces with the anode, and in support of this it has been shown that the V_{OC} in such cells can be manipulated in a systematic fashion using electrolytes of different potential, producing values of up to 200 mV in cells with RC-LH1 complexes [43]. A drawback of this device architecture, however, is the possibility that the mediator can enable futile recombination of electrons between the reducing and oxidising terminals of the RC (dotted arrow in Figure 1b), negatively affecting both the photocurrent and photovoltage. In addition, it is possible that such a mediator could also facilitate electron flow from the FTO cathode to P^+. In such a scenario, with the same mediator interfacing the photoprotein with both electrodes, the V_{OC} would be expected to be very low.

In the present report we explore a new strategy in which light-induced charge separation in RC-LH1 complexes adhered to a FTO-glass cathode was connected to a second photo-transition in an n-doped silicon (n-Si) anode in a sandwich-style, two electrode device architecture. Illumination of n-Si produces holes in its valence band at a potential much more oxidising than the P/P^+ couple in the RC. The protein/FTO cathode and n-Si anode were connected by an electrolyte solution containing either the nitroxide-containing organic radical 2,2,6,6-tetramethyl-1-piperidinyloxy (TEMPO), the metallocene couple ferrocene/ferrocenium, or the iodide/triiodide (I^-/I_3^-) couple commonly used in dye-sensitized solar cells. Each of these electrolytes has a potential considerably more oxidising than P/P^+, and so cannot mediate unwanted electron transfer between the reducing and oxidising terminals

of the RC protein or between the protein and the cathode. In addition, we evaluated both planar silicon and silicon that had been textured with micrometre scale pyramidal surface structure to increase the electrode area and reduce photon reflection. We find that such cells exhibit open circuit voltages of up to 700 mV under illumination. The basis of the high voltages generated by these novel biohybrid cells is discussed.

Results and Discussions

Before construction of photoelectrochemical cells the redox energy levels of the three electrolytes were determined by cyclic voltammetry (Figure 2a). In good agreement with reported values[44], ferrocene and TEMPO each had one redox pair at 0.63 V and 0.87 V (*vs.* NHE), respectively. The iodide/triiodide system had two redox pairs at 0.71 V and 0.79 V, the first of which corresponded to the I^-/I_3^- couple. TEMPO possessed the highest redox potential relative to that for oxidation of the RC primary electron donor, followed by I^-/I_3^- and ferrocene. Equivalent vacuum potentials are compiled in Table 1.

RC-LH1 cells were fabricated by drop casting 4 μL of protein solution onto a cleaned FTO surface followed by vacuum drying to produce a protein film (see Methods). The electrolyte solution was then dropped onto the protein film, and the back electrode brought in contact. The current and voltage outputs of the three types of cell were measured without any applied bias (see Methods). With 0.2 M ferrocene, a steady-state photo-induced V_{OC} of ≈320 mV was obtained (Figure 2b), over and above a dark voltage of -50 mV (see Table S1 in Supporting Information). This was accompanied by a peak transient J_{sc} of -8.8 μA/cm^2 that decayed in a couple of seconds to a lower steady-state value of ≈-0.3 μA/cm^2 (Figure 2c). Such decays have been previously attributed to limitations imposed by electrolyte diffusion[20, 40, 45, 46] and this has been confirmed experimentally[19]. Cells fabricated with 0.2 M I^-/I_3^- as electrolyte produced a steady-state photo-induced V_{OC} of ≈460 mV (Figure 2b and Table S1) and a peak J_{SC} of -3.0 μA/cm^2 that decayed to a low steady state level of ~-0.1 μA/cm^2 (Figure 2c). With 0.2 M TEMPO, cells produced a steady state photo-induced V_{OC} of around 620 mV (Figure 2b and Table S1) and a peak J_{SC} of ≈-7.7 μA/cm^2 that decayed to a steady-state photocurrent of ≈-1.1 μA/cm^2 (Figure 2c). As is evident from the data compiled in Table 1 both the peak and steady-state J_{SC} did not show any dependence on the vacuum potential of the electrolyte, as might be expected, but the photo-induced V_{OC} increased as the electrolyte became more

oxidising, in an approximately linear fashion (Table 1). The time taken for the V_{OC} to stabilise also increased as the electrolyte became more oxidising; the likely reason for this is discussed below.

In this cell architecture the photoprotein effectively creates an electric potential to drive electrons out of the n-Si wafer used as the anode. To confirm that the RC-LH1 complexes were the source of the observed photoresponses an external quantum efficiency (EQE) action spectrum was recorded for a TEMPO cell and compared to the absorbance spectrum of the RC-LH1 complex in solution (Figure 2d). The absorbance spectrum showed a dominant absorbance band at 874 nm, attributable to the 32 BChl light harvesting pigments of the LH1 antenna protein and the pair of P BChls of the RC, and a band at 805 nm attributable to the two monomeric BChls of the RC. The EQE spectrum had a maximum of 1.0 % at 860 nm and the positions of its bands corresponded reasonably well with absorption spectrum of the RC-LH1 complex in solution. In addition to confirming that the RC-LH1 complex was responsible for driving the photocurrent, the line shape of the EQE spectrum provided insight into factors limiting that photocurrent. The low amplitude of the longest wavelength band in the EQE spectrum, attributable (mainly) to the LH1 BChls (i.e. 875 nm absorption peak), relative to the adjacent band at 805 nm attributable to the RC indicated the likelihood that the photocurrent is not limited by light harvesting by the antenna pigments. This response characteristic has been observed previously in photoelectrochemical cells employing RC-LH1 complexes and its origin discussed[22].

A power conversion efficiency (η) for each of the cells was estimated by multiplying the J_{SC} by the V_{OC} and dividing by the incident light intensity of 100 mW/cm^2 (Table 1). This modified method was used as it was not possible to determine a fill factor from a full I-V curve due to the transient nature of the photocurrents (see ref[47] for a previous discussion). The highest value of η was obtained with TEMPO, which gave the highest V_{OC} and J_{SC}, and the lowest η was with I^-/I_3^- which gave the lowest J_{SC} (Table 1).

The function of the oxidising electrolytes was to shuttle charge from the protein adhered to the FTO-glass electrode to the n-Si counter electrode. To better understand the electrochemical characteristics of the n-Si/electrolyte interaction electrochemical impedance spectroscopy (EIS) was performed on symmetrical cells. The Nyquist plots (Figure 3a) were obtained from the symmetrical cells fabricated by sandwiching an aliquot of electrolyte solution between two identical n-Si wafers (Figure 3b). The modelled equivalent circuit used

for data fitting is shown in Figure 3c. Typically, the high frequency range of the impedance curve is attributed to the series resistance (R_s) which includes the bulk resistance of the counter electrode and the contact resistance. The middle frequency range can be assigned to the resistance capacitance networks of the electrode/electrolyte interface. This includes the charge transfer resistance (R_{ct}) which refers to the barrier through which the electron must pass between the electrode surface and the adsorbed species, and is a measure of the rate of electron exchange between the redox electrolyte and the counter electrode. The low frequency range can be assigned to the diffusion impedance of the redox electrolyte.

The diameters of the semicircles in the Nyquist plots provide a good way to compare the charge transfer resistance as the smaller the semicircle, the lower the charge transfer resistance and the faster charge transfer kinetics. As seen from Figure 3a, symmetrical cells with ferrocene had a much larger charge transfer resistance than cells with I^-/I^-_3 or TEMPO. Despite the similar, low charge transfer resistances obtained for I^-/I^-_3 and TEMPO, the steady-state photocurrent obtained with I^-/I^-_3 was eleven-fold lower than that obtained with TEMPO. This is attributed to the irreversibility of the redox process associated with the I^-/I^-_3 electrolyte (Figure 2a). Although the first redox curve in the I^-/I^-_3 CV trace can be described by the process $3\ I^- \leftrightarrow 3\ I^- + 2\ e^-$, there was no reduction of I^-_3 back to I^- in γ-butyrolactone (Figure 2a). Were the same to be the case in the protein photoelectrochemical cells then the oxidation of the Q_B ubiquinone would be inhibited, breaking the electronic circuit and stopping charge flow, resulting in a poor photocurrent. The observation that the photocurrent obtained with ferrocene was also lower than that obtained with TEMPO can be attributed to the high charge transfer resistance associated with ferrocene.

As mentioned above, the time required for stabilisation of the photo-induced V_{OC} depended on the electrolyte used (Figure 2b). For ferrocene, which gave the lowest final V_{OC}, attainment of a steady value was very rapid. In contrast for TEMPO, which gave the highest final V_{OC}, stabilisation took around 300 seconds (see inset to Figure 2b), with an intermediate result for iodide. The most likely explanation is that this was a consequence of the size of the energy-level difference between the quinone Q_B site of the protein and the electrolyte. For TEMPO, the deepest lying redox electrolyte, electron-transfer might be expected to be slowest because this energy gap was the largest, resulting in a gradual build-up of photovoltage over 200-300 seconds. For iodide and ferrocene the build-up was more rapid because the energy gap

between the Q_B and electrolyte was smaller, being most rapid for ferrocene where the energy gap was smallest and the steady state was reached within ≈1 s.

To explore the possibility of further improving cell performance the n-Si counter electrode was textured to produce micrometer scale pyramidal structures at its surface (Figure 4a). Protein photoelectrochemical cells were constructed with TEMPO as the electrolyte and with either flat or textured n-Si as the back electrode. Allowing for a dark voltage of 210 mV, a photo-induced V_{OC} of ≈700 mV was obtained from RC-LH1 cells with a textured back electrode (Figure 4b and Table S1), a ≈13% improvement over that obtained with planar n-Si. The amplitude of the steady-state photocurrent density from the textured n-Si cells was eight-fold larger than that obtained with planar Si (Figure 4c and Table 2). The dark current exhibited by the cells with a textured n-Si anode was not seen for cells with a planar electrode (Figure 4b) and likely arose from trapped charges at the textured silicon surface.

Replacing planar n-Si with textured n-Si gave a ≈eight fold increase in power conversion efficiency (Table 2). This is principally attributed to enhanced charge transfer and enhanced light absorption by the n-Si. To corroborate the first of these, EIS was performed on the protein cells used for photocurrent and photovoltage measurements. The EIS spectra (Figure 4d) obtained from the protein cells (Figure 4e) were fitted using an equivalent circuit model (Figure 4f, Figure S1). The equivalent circuit model is chosen based on the impedance characteristics of the individual components in the cell (Figure S1). However, as it is seen that the circuit model fitted still shows minor deviations from the EIS Nyquist spectra, a more profound physical understanding of the solid-state protein layers and their interactions with electrolytes is needed to arrive at a circuit model with a better fit. The fitted Nyquist plots revealed a seven-fold drop in charge transfer resistance R_{ct} when the plain Si was replaced with textured Si (Table 2). It is likely that this was due to the increase in the interfacial area between the electrode and the electrolyte. Regarding the second effect, it is well known that texturing the Si surface with random pyramidal structures minimizes reflection losses (Fig. 4g) and so enhances light absorption by the Si.

The proposed mechanism of photo-induced charge transfer in the biohybrid cells is illustrated in the energy diagram in Figure 5. Illumination of the RC-LH1 protein oxidises the special pair bacteriochlorophylls (P^+) and reduces the terminal ubiquinone (Q_B^-), with P^+ being re-reduced by the FTO-electrode in a process that would not be expected to involve any of the three evaluated deep-lying electrolytes. In parallel, light not absorbed by the protein layer

triggers a photoexcitation in n-Si generating an electron-hole pair. The hole in the valence band is subsequently filled by the electrolyte, completing the circuit. In this novel architecture the maximum possible V_{OC} is determined by the potential gap between the P/P^+ couple in the photoprotein, at -5.0 eV, and the conduction band of the n-Si at ~-4.3 eV, a span of around 0.7 eV which is good agreement with the photovoltage observed in the cell with a textured n-Si counter electrode and the deepest lying TEMPO electrolyte. In addition to providing a means of shuttling electrons between the protein and the n-Si, the use of electrolytes with deep-lying vacuum potentials avoided the possibility of the electrolyte facilitating short-circuit electron flow between the Q_B^- and P^+ terminals of the protein, or being involved in electron flow from the FTO-glass cathode to P^+.

Regarding overall cell performance, a point to note is that the simple approach taken to fabrication of the working electrode in these cells, vacuum drying a protein layer directly onto a cleaned but unfunctionalised FTO-glass surface, did not provide a mechanism to control protein orientation at the electrode surface. The orientation depicted in Figures 1 and 5, with the side of the protein normally exposed to the bacterial periplasm closest to the FTO-surface, places the P/P^+ redox center closest to the FTO-glass to support a cathodic photocurrent. This part of the protein surface is very flat, and the P bacteriochlorophylls are located close to the surface. However, it is likely that proteins in the vacuum dried layer are oriented more randomly than this, and that this is a factor that limits the magnitude of the photocurrents produced by these devices. For example, proteins oriented with their cytoplasmic side closest to the FTO could support an anodic current through electron donation from the RC quinones, such that the observed photocurrent is the sum of cathodic and anodic processes. It should be noted that the protein surface on the cytoplasmic side of the membrane is more strongly contoured than on the periplasmic side due to the presence of the H domain of the RC (coloured as a pink solid surface in Figures 1 and 5). Also, the quinones are more deeply buried in the protein interior than is the case for the P bacteriochlorophylls, as the function of the H domain is to insulate the quinone binding site from the extramembrane aqueous phase.

Another factor that we cannot rule out is some detachment of individual proteins from the vacuum dried layer during cell assembly and performance, although these vacuum dried protein films were reasonably resistant to rinsing using deionised water. Although free protein in solution would not be expected to support a photocurrent, it could affect cell performance by adhering to the counter electrode and so interfering with electrode/electrolyte interactions. In future work, therefore, it may be possible to boost the photocurrent from this type of device

through better control of protein orientation and adherence at the working electrode, although this would have the trade-off of making cell fabrication more complex. In addition, the mechanisms through which protein multilayers support photocurrents are poorly understood, particularly with regard to those proteins not in immediate contact with either electrode or electrolyte, and a better understanding of this architecture should also enable improvements in cell design to boost output.

In conclusion, high photovoltages have been achieved through a device design incorporating two parallel photoexcitation reactions at a FTO-glass/protein cathode and an n-doped silicon anode. The highest V_{OC} of ~0.7 V was obtained with the deepest lying electrolyte, TEMPO, in conjunction with a textured n-Si anode, producing a power conversion efficiency of 5.7×10^{-3} %. This raises the photovoltage achievable in a device employing purple bacterial photoproteins to a level comparable to that typical of silicon heterojunction and dye-sensitized solar cells. The challenge now is to seek mechanisms to enhance the photocurrent achievable in such cells to similarly raise the power conversion efficiency of these biohybrid devices.

Methods

RC-LH1 cell fabrication and characterization

Conductive FTO-glass (TEC 15 Ω/sq; MTI Corporation, USA) was used as the transparent front electrode and was cleaned by sonication in acetone and then in isopropanol. The back electrode was a high-purity prime grade n-doped silicon wafer (Latech Scientific Supply Pte. Ltd.) with a resistivity of 10 Ω·cm. The etching procedure for the textured Si wafer can be found elsewhere[48]. Electrolyte solutions comprised 0.2 M ferrocene, TEMPO or iodide/triiodide in γ-butyrolactone. RC-LH1 complexes lacking the PufX protein were purified as described previously[25] and stored at −80 °C as a concentrated solution in 20 mM Tris (pH 8.0)/0.04 % (w/v) DDM. To fabricate all RC-LH1 cells a 4 μL aliquot of protein solution was pipetted onto the cleaned FTO substrate and vacuum dried to produce a dry protein film. A 6 μL aliquot of electrolyte solution was pipetted onto the protein film and the back electrode was brought in contact. Cell assembly was completed by fixing the two electrodes in place using binder clips and the sides were sealed with epoxy resin.

Photochronoamperometry was performed using a tungsten-halogen light source with a light intensity of 100 mW/cm^2 on an active area 0.04 cm^2. All measurements were performed using a K2400 source meter (Keithley). For EQE measurements, light from a quartz tungsten halogen lamp was dispersed through a monochromator and the output focused onto the cell.

Cyclic voltammetry

Redox potentials of the electrolytes as 10 mM solutions were determined using an Autolab electrochemical workstation (Metrohm). Glassy carbon was used as the working electrode, Ag/AgCl (3 M KCl) was used as the reference electrode and a platinum wire was used as the counter electrode. The supporting electrolyte solution consisted of 0.1 M lithium perchlorate in γ-butyrolactone.

Electrochemical impedance measurements

Impedance measurements were performed with a computer-controlled Autolab potentiostat (Metrohm) equipped with a frequency response analyser. The magnitude of the alternative signal was 10 mV. Symmetrical cells for impedance measurements were formed from two n-Si electrodes with an active surface area of 1 cm^2. Redox electrolytes were the same as those used in fabrication of RC-LH1 cells.

Acknowledgements

S.C.T. acknowledges the financial support from MOE AcRF 1 (R-284-000-134-112 and R-284-000-129-133). M.R.J. acknowledges support from the Biotechnology and Biological Sciences Research Council of the UK (project BB/I022570/1).

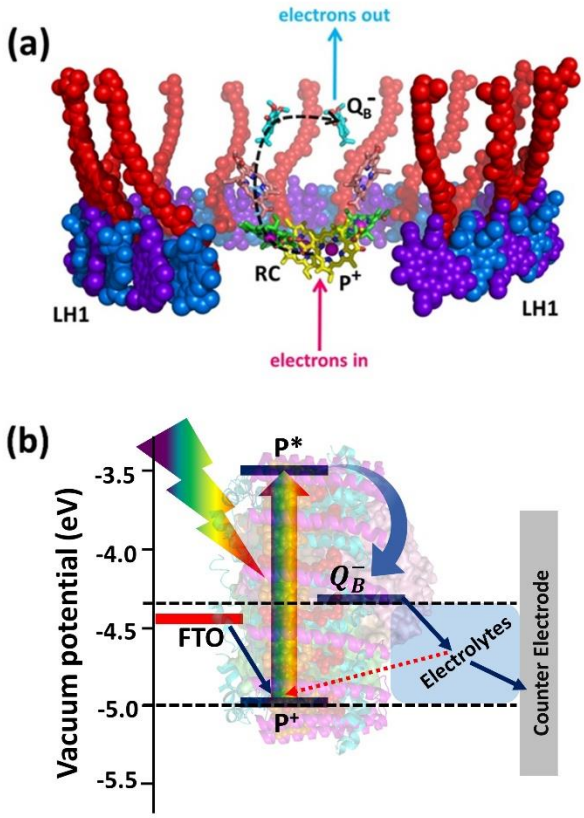

Figure 1. **General mechanism of charge separation and photovoltage generation by RC-LH1 complexes in a sandwich-configuration biohybrid cell.** (a) View of the cofactors of the RC-LH1 complex with the six nearest LH1 cofactors removed. The LH1 light harvesting pigments comprise 32 BChls (alternating blue/purple) and 16 carotenoids (red). Energy transfer to the P BChls of the RC (yellow sticks) triggers charge separation (dotted arrow) through the RC cofactors (sticks) to the terminal Q_B ubiquinone acceptor (cyan sticks). After charge separation to form $P^+Q_B^-$, electrons enter the complex through reduction of P^+ (magenta arrow) and leave the complex through oxidation of Q_B^- (cyan arrow). It should be noted that in some device configurations current flow may be dependent on double reduction and protonation of Q_B to form Q_BH_2; for simplicity this is not shown or discussed in the text. (b) Mechanism of photocurrent generation in a photoelectrochemical cell in which RC-LH1 (or RC) proteins interface directly with a FTO-glass anode and a diffusing electrolyte carries charge to the anode. The V_{OC} is determined by the potential gap between the P/P^+ redox couple in the protein and the electrolyte. With electrolytes that have potentials intermediate between those of P/P^+ and Q_B/Q_B^- there is also the possibility that they will carry charge to P^+ from either the FTO electrode or from Q_B^-, affecting the observed V_{OC}.

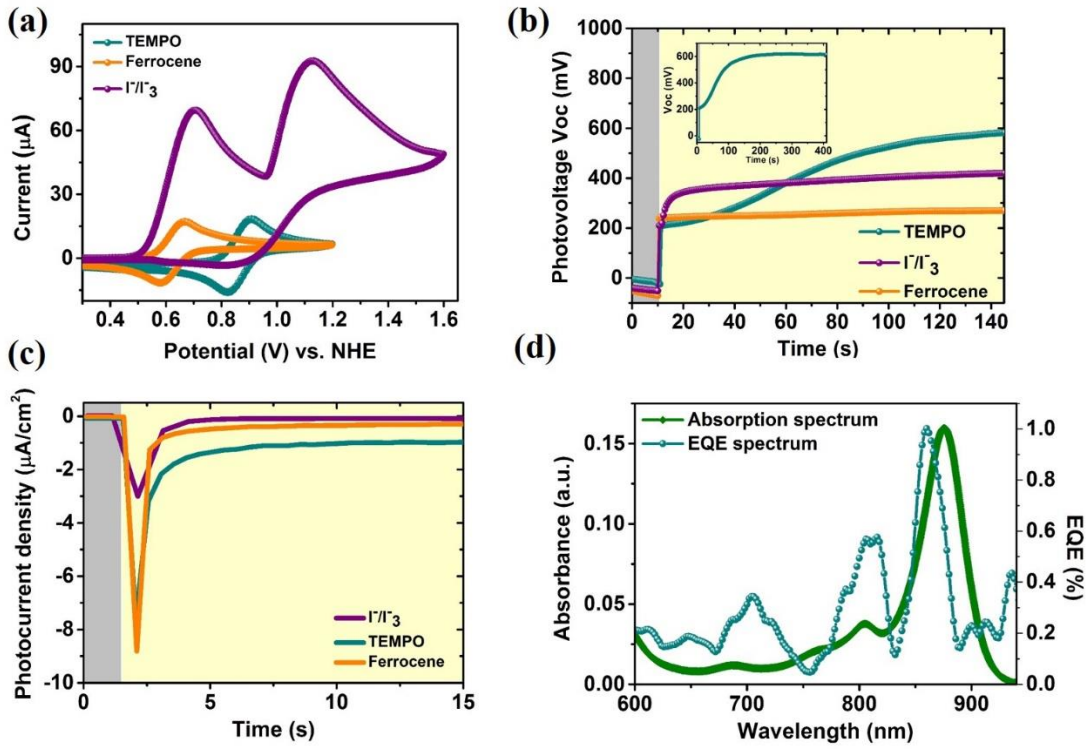

Figure 2. **Cell components and performance.** (a) Cyclic voltammograms of the three electrolytes tested. Each was a 10 mM solution in γ-butyrolactone with 0.1 M lithium perchlorate, recorded at a scan rate of 100 mV/s. (b) *V*oc (Inset: steady-state photovoltage in TEMPO cell over 400 s) and (c) *J*sc produced by RC-LH1 cells with different electrolytes under illumination. (d) Absorbance spectrum of RC-LH1 proteins in solution compared with an EQE action spectrum for an RC-LH1 cell with TEMPO.

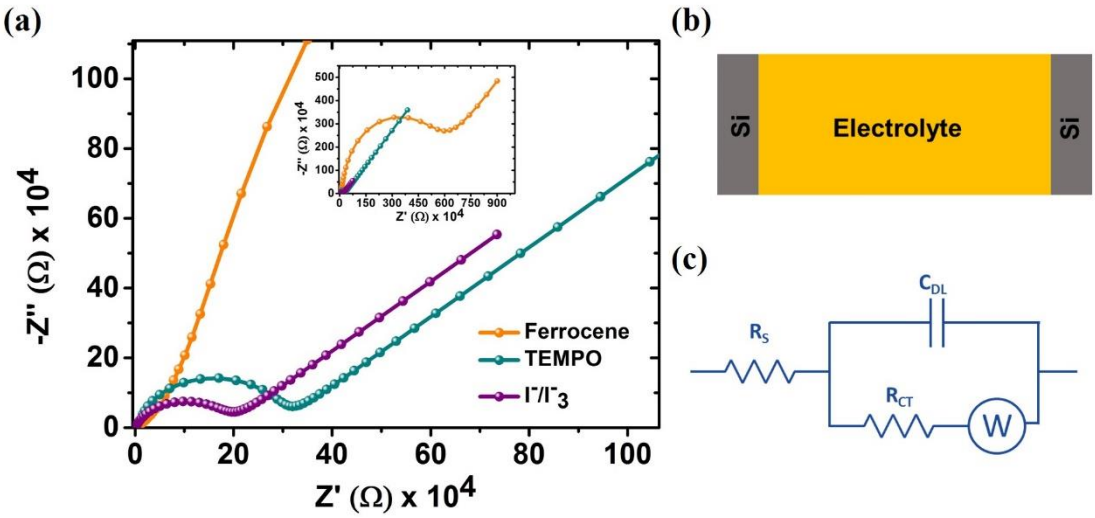

Figure 3. Interactions of the electrolytes with the planar n-Si electrode. (a) Nyquist plots of EIS data for symmetrical cells using different electrolytes. The inset shows the complete EIS spectrum obtained. (b) Schematic of the symmetrical cells. (c) Equivalent circuit model used to fit the impedance spectra of symmetrical cells.

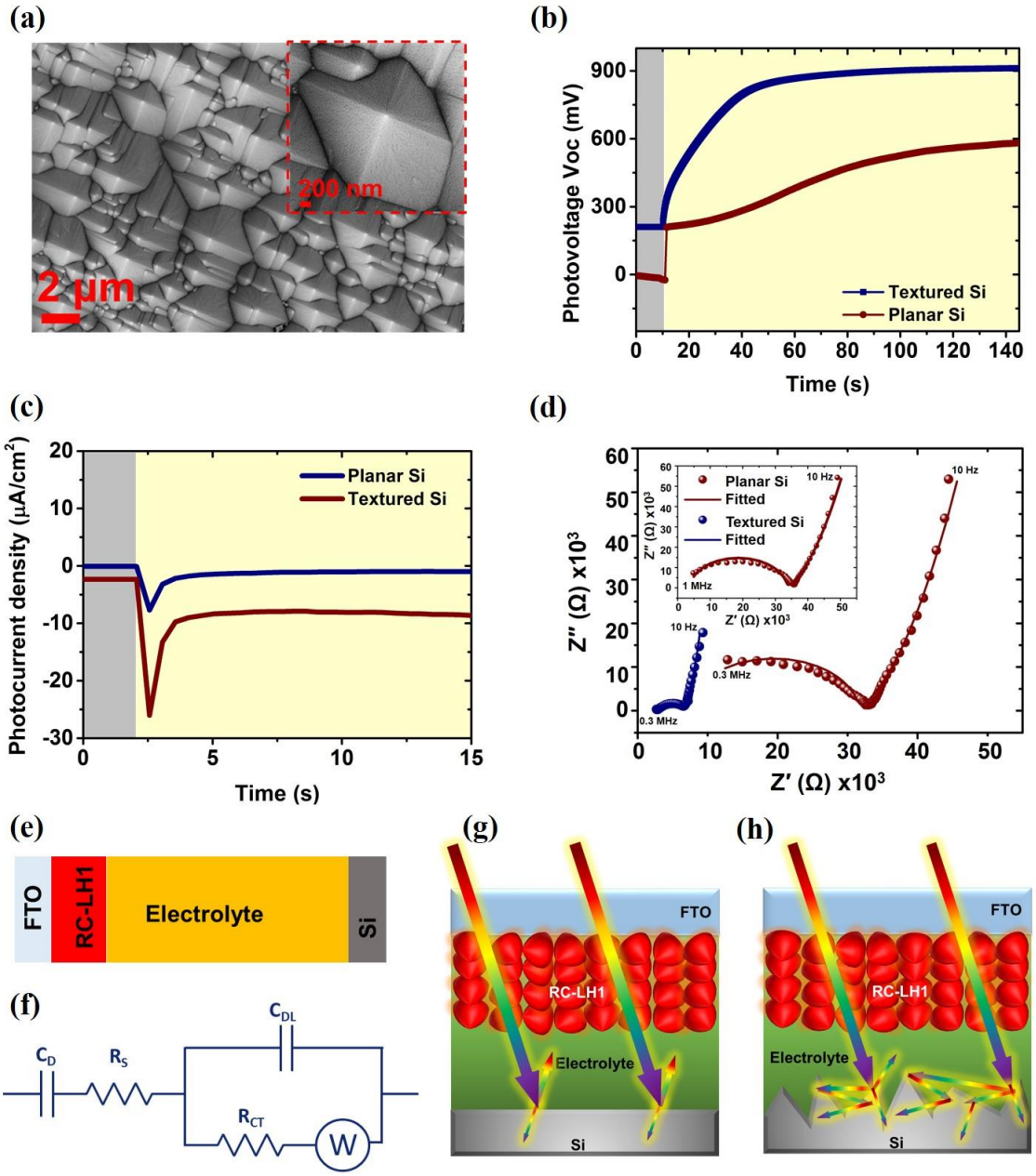

Figure 4. Voltage and current enhancements from texturing the silicon counter electrode. (a) Scanning electron microscopy image of the textured n-Si electrode showing pyramidal structures. (b) V_{OC} and (c) J_{SC} from RC-LH1 cells with 0.2 M TEMPO as electrolyte and a planar or textured Si counter electrode. (d) Nyquist plots of EIS data for these cells over the frequency range 10 Hz to 0.3 MHz. The inset shows the complete EIS spectrum for the cell with a plain n-Si electrode with the frequency range extended to 1 MHz. (e) Schematic of the RC-LH1 cells. (f) Equivalent circuit model used for fitting the impedance spectra of the cells. (g) In cells formed from planar Si a significant portion of the incoming light is reflected back into electrolyte. (h) Enhanced light absorption by a textured n-Si electrode occurs because the

pyramidal structures scatter light back to the surface enabling multiple instances of absorption and producing minimal reflection.

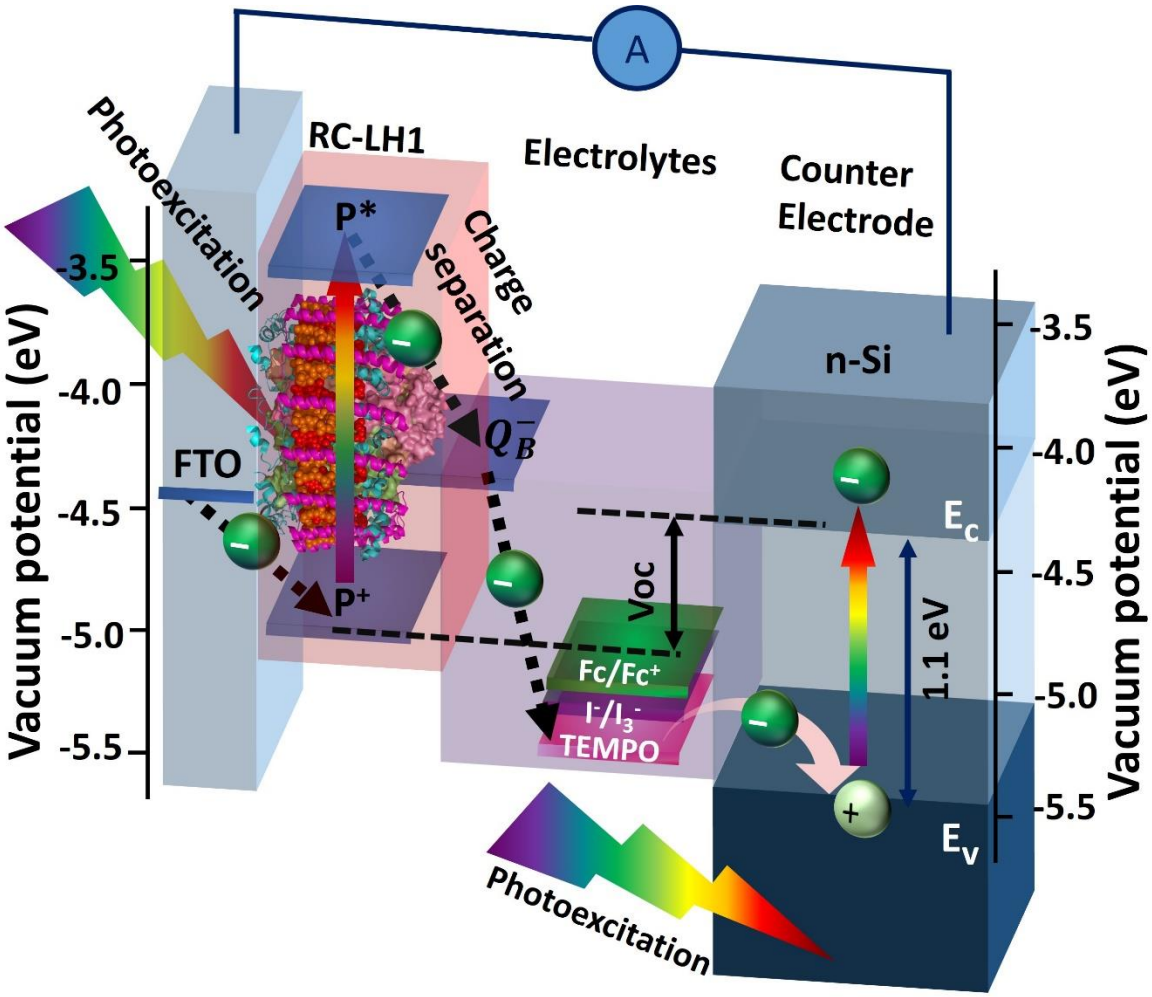

Figure 5. Schematic of charge transport through the biohybrid cell. Incident light triggers a primary photochemical reaction in the RC-LH1 complex involving photoexcitation of the special pair (P→P*) and charge separation to form P^+ and Q_B^-. Unabsorbed light triggers auxiliary photoexcitation in n-Si resulting in excitation of an electron into the conduction band (E_C) and leaving a hole in the valence band (E_V). The two photo-reactions are coupled by the electrolytes with deep-lying vacuum potentials which fill holes in the n-Si valence band using electrons collected from the Q_B^- cofactors in the RC-LH1 complex.

Table 1. Photovoltaic performance of the RC-LH1 cells with different electrolytes and a planar n-Si counter electrode.

Electrolyte	Electrolyte vacuum potential (eV)	J_{sc} ($\mu A/cm^2$)	V_{oc}[a] (mV)	η[b] (%) x 10^{-3}
$TEMPO/TEMPO^+$	-5.35	1.1	620	0.68
I^-/I^-_3	-5.21	0.1	460	0.05
Fc/Fc^+	-5.13	0.3	320	0.10

[a]Values refer to the photo-induced changes in V_{oc} (i.e. light voltage – dark voltage). Refer to Table S1

[b]The power conversion efficiencies (η) of the cells were estimated from $\eta = \frac{Jsc \times Voc}{P_{in}} \times 100$ without considering fill factors due to the transient nature of photocurrent. P_{in} = 100 mW/cm^2)

Table 2. Photovoltaic performance and charge conduction for RC-LH1/TEMPO cells with a planar or textured n-Si electrodes

Anode	V_{oc} (mV)	J_{sc} ($\mu A/cm^2$)	η (%) x 10^{-3}	R_s (kΩ)	R_{ct} (kΩ)
Planar Si	620	1.1	0.68	7.5	23.7
Textured Si	700	8.2	5.75	2.9	3.2

References:

1. LaVan DA, Cha JN. Approaches for biological and biomimetic energy conversion. *Proceedings of the National Academy of Sciences* 2006, **103**(14)**:** 5251-5255.

2. Badura A, Kothe T, Schuhmann W, Rogner M. Wiring photosynthetic enzymes to electrodes. *Energy & Environmental Science* 2011, **4**(9)**:** 3263-3274.

3. Boghossian AA, Ham M-H, Choi JH, Strano MS. Biomimetic strategies for solar energy conversion: a technical perspective. *Energy & Environmental Science* 2011, **4**(10)**:** 3834-3843.

4. Wang F, Liu X, Willner I. Integration of Photoswitchable Proteins, Photosynthetic Reaction Centers and Semiconductor/Biomolecule Hybrids with Electrode Supports for Optobioelectronic Applications. *Advanced Materials* 2013, **25**(3)**:** 349-377.

5. Kim Y, Shin SA, Lee J, Yang KD, Nam KT. Hybrid system of semiconductor and photosynthetic protein. *Nanotechnology* 2014, **25**(34)**:** 342001.

6. Khoa N, Bruce BD. Growing green electricity: Progress and strategies for use of Photosystem I for sustainable photovoltaic energy conversion. *Biochimica Et Biophysica Acta-Bioenergetics* 2014, **1837**(9)**:** 1553-1566.

7. Yehezkeli O, Tel-Vered R, Michaeli D, Willner I, Nechushtai R. Photosynthetic reaction center-functionalized electrodes for photo-bioelectrochemical cells. *Photosynthesis research* 2014, **120**(1-2)**:** 71-85.

8. Operamolla A, Ragni R, Milano F, Roberto Tangorra R, Antonucci A, Agostiano A*, et al.* "Garnishing" the photosynthetic bacterial reaction center for bioelectronics. *Journal of Materials Chemistry C* 2015, **3**(25)**:** 6471-6478.

9. Ravi SK, Tan SC. Progress and perspectives in exploiting photosynthetic biomolecules for solar energy harnessing. *Energy & Environmental Science* 2015, **8**(9)**:** 2551-2573.

10. Carmeli I, Frolov L, Carmeli C, Richter S. Photovoltaic Activity of Photosystem I-Based Self-Assembled Monolayer. *Journal of the American Chemical Society* 2007, **129**(41)**:** 12352-12353.

11. Gizzie EA, Scott Niezgoda J, Robinson MT, Harris AG, Kane Jennings G, Rosenthal SJ*, et al.* Photosystem I-polyaniline/TiO2 solid-state solar cells: simple devices for biohybrid solar energy conversion. *Energy & Environmental Science* 2015, **8**(12)**:** 3572-3576.

12. Shah VB, Henson WR, Chadha TS, Lakin G, Liu H, Blankenship RE*, et al.* Linker-Free Deposition and Adhesion of Photosystem I onto Nanostructured TiO2 for Biohybrid Photoelectrochemical Cells. *Langmuir* 2015, **31**(5)**:** 1675-1682.

13. Stieger KR, Feifel SC, Lokstein H, Hejazi M, Zouni A, Lisdat F. Biohybrid architectures for efficient light-to-current conversion based on photosystem I within scalable 3D mesoporous electrodes. *Journal of Materials Chemistry A* 2016, **4**(43)**:** 17009-17017.

14. Kothe T, Plumeré N, Badura A, Nowaczyk MM, Guschin DA, Rögner M*, et al.* Combination of A Photosystem 1-Based Photocathode and a Photosystem 2-Based Photoanode to a Z-Scheme Mimic for Biophotovoltaic Applications. *Angewandte Chemie International Edition* 2013, **52**(52)**:** 14233-14236.

15. LeBlanc G, Chen G, Gizzie EA, Jennings GK, Cliffel DE. Enhanced Photocurrents of Photosystem I Films on p-Doped Silicon. *Advanced Materials* 2012, **24**(44)**:** 5959-5962.

16. Mahmoudzadeh A, Saer R, Jun D, Mirvakili SM, Takshi A, Iranpour B*, et al.* Photocurrent generation by direct electron transfer using photosynthetic reaction centres. *Smart Materials & Structures* 2011, **20**(9).

17. Yaghoubi H, Lafalce E, Jun D, Jiang X, Beatty JT, Takshi A. Large Photocurrent Response and External Quantum Efficiency in Biophotoelectrochemical Cells Incorporating Reaction Center Plus Light Harvesting Complexes. *Biomacromolecules* 2015, **16**(4)**:** 1112-1118.

18. Kamran M, Delgado JD, Friebe V, Aartsma TJ, Frese RN. Photosynthetic Protein Complexes as Bio-photovoltaic Building Blocks Retaining a High Internal Quantum Efficiency. *Biomacromolecules* 2014, **15**(8)**:** 2833-2838.

19. Friebe VM, Delgado JD, Swainsbury DJ, Gruber JM, Chanaewa A, van Grondelle R*, et al.* Plasmon-Enhanced Photocurrent of Photosynthetic Pigment Proteins on Nanoporous Silver. *Advanced Functional Materials* 2016, **26**(2)**:** 285-292.

20. Tan SC, Crouch LI, Jones MR, Welland M. Generation of Alternating Current in Response to Discontinuous Illumination by Photoelectrochemical Cells Based on Photosynthetic Proteins. *Angewandte Chemie-International Edition* 2012, **51**(27)**:** 6667-6671.

21. Tan SC, Yan F, Crouch LI, Robertson J, Jones MR, Welland ME. Superhydrophobic Carbon Nanotube Electrode Produces a Near-Symmetrical Alternating Current from Photosynthetic Protein-Based Photoelectrochemical Cells. *Advanced Functional Materials* 2013, **23**(44)**:** 5556-5563.

22. den Hollander M-J, Magis JG, Fuchsenberger P, Aartsma TJ, Jones MR, Frese RN. Enhanced Photocurrent Generation by Photosynthetic Bacterial Reaction Centers through Molecular

Relays, Light-Harvesting Complexes, and Direct Protein-Gold Interactions. *Langmuir* 2011, **27**(16)**:** 10282-10294.

23. Yu D, Wang M, Zhu G, Ge B, Liu S, Huang F. Enhanced photocurrent production by bio-dyes of photosynthetic macromolecules on designed TiO2 film. *Scientific Reports* 2015, **5:** 9375.

24. Friebe VM, Swainsbury DJK, Fyfe PK, van der Heijden W, Jones MR, Frese RN. On the mechanism of ubiquinone mediated photocurrent generation by a reaction center based photocathode. *Biochimica et Biophysica Acta (BBA) - Bioenergetics* 2016, **1857**(12)**:** 1925-1934.

25. Ravi SK, Yu Z, Swainsbury DJK, Ouyang J, Jones MR, Tan SC. Enhanced Output from Biohybrid Photoelectrochemical Transparent Tandem Cells Integrating Photosynthetic Proteins Genetically Modified for Expanded Solar Energy Harvesting. *Advanced Energy Materials* 2016**:** 1601821-n/a.

26. Das R, Kiley PJ, Segal M, Norville J, Yu AA, Wang LY*, et al.* Integration of photosynthetic protein molecular complexes in solid-state electronic devices. *Nano Letters* 2004, **4**(6)**:** 1079-1083.

27. Yaghoubi H, Schaefer M, Yaghoubi S, Jun D, Schlaf R, Beatty JT*, et al.* A ZnO nanowire bio-hybrid solar cell. *Nanotechnology* 2017, **28**(5)**:** 054006.

28. Terasaki N, Yamamoto N, Tamada K, Hattori M, Hiraga T, Tohri A*, et al.* Bio-photosensor: Cyanobacterial photosystem I coupled with transistor via molecular wire. *Biochimica et Biophysica Acta (BBA) - Bioenergetics* 2007, **1767**(6)**:** 653-659.

29. Chatzipetrou M, Milano F, Giotta L, Chirizzi D, Trotta M, Massaouti M*, et al.* Functionalization of gold screen printed electrodes with bacterial photosynthetic reaction centres by laser printing technology for mediatorless herbicide biosensing. *Electrochemistry Communications* 2016, **64:** 46-50.

30. Swainsbury DJ, Friebe VM, Frese RN, Jones MR. Evaluation of a biohybrid photoelectrochemical cell employing the purple bacterial reaction centre as a biosensor for herbicides. *Biosensors and Bioelectronics* 2014, **58:** 172-178.

31. Oliver JWK, Atsumi S. Metabolic design for cyanobacterial chemical synthesis. *Photosynthesis Research* 2014, **120**(3)**:** 249-261.

32. Croce R, van Amerongen H. Natural strategies for photosynthetic light harvesting. *Nature chemical biology* 2014, **10**(7)**:** 492-501.

33. Scholes GD, Fleming GR, Olaya-Castro A, van Grondelle R. Lessons from nature about solar light harvesting. *Nature chemistry* 2011, **3**(10)**:** 763-774.

34. Feher G, Allen JP, Okamura M, Rees D. Structure and function of bacterial photosynthetic reaction centres. *Nature* 1989, **339:** 111-116.

35. Zinth W, Wachtveitl J. The first picoseconds in bacterial photosynthesis - Ultrafast electron transfer for the efficient conversion of light energy. *Chemphyschem* 2005, **6**(5)**:** 871-880.

36. Jones MR. The petite purple photosynthetic powerpack. *Biochemical Society Transactions* 2009, **37:** 400-407.

37. Niwa S, Yu L-J, Takeda K, Hirano Y, Kawakami T, Wang-Otomo Z-Y*, et al.* Structure of the LH1-RC complex from Thermochromatium tepidum at 3.0 [thinsp] A. *Nature* 2014, **508**(7495)**:** 228-232.

38. Qian P, Papiz MZ, Jackson PJ, Brindley AA, Ng IW, Olsen JD*, et al.* Three-Dimensional Structure of the Rhodobacter sphaeroides RC-LH1-PufX Complex: Dimerization and Quinone Channels Promoted by PufX. *Biochemistry* 2013, **52**(43)**:** 7575-7585.

39. Blankenship RE. *Molecular mechanisms of photosynthesis*. John Wiley & Sons, 2013.

40. Takshi A, Madden JD, Beatty JT. Diffusion model for charge transfer from a photosynthetic reaction center to an electrode in a photovoltaic device. *Electrochimica Acta* 2009, **54**(14)**:** 3806-3811.

41. Lu YD, Yuan MJ, Liu Y, Tu B, Xu CH, Liu BH*, et al.* Photoelectric performance of bacteria photosynthetic proteins entrapped on tailored mesoporous WO3-TiO2 films. *Langmuir* 2005, **21**(9)**:** 4071-4076.

42. Xu J, Lu Y, Liu B, Xu C, Kong J. Sensitively probing the cofactor redox species and photo-induced electron transfer of wild-type and pheophytin-replaced photosynthetic proteins reconstituted in self-assembled monolayers. *Journal of Solid State Electrochemistry* 2007, **11**(12)**:** 1689-1695.

43. Tan SC, Crouch LI, Mahajan S, Jones MR, Welland ME. Increasing the Open-Circuit Voltage of Photoprotein-Based Photoelectrochemical Cells by Manipulation of the Vacuum Potential of the Electrolytes. *Acs Nano* 2012, **6**(10)**:** 9103-9109.

44. Jeena V, Robinson RS. Convenient photooxidation of alcohols using dye sensitised zinc oxide in combination with silver nitrate and TEMPO. *Chemical Communications* 2012, **48**(2)**:** 299-301.

45. Caterino R, Csiki R, Lyuleeva A, Pfisterer J, Wiesinger M, Janssens SD*, et al.* Photocurrent generation in diamond electrodes modified with reaction centers. *ACS applied materials & interfaces* 2015, **7**(15)**:** 8099-8107.

46. Katz E. Application of bifunctional reagents for immobilization of proteins on a carbon electrode surface: oriented immobilization of photosynthetic reaction centers. *Journal of Electroanalytical Chemistry* 1994, **365**(1-2)**:** 157-164.

47. Ciesielski PN, Hijazi FM, Scott AM, Faulkner CJ, Beard L, Emmett K*, et al.* Photosystem I – Based biohybrid photoelectrochemical cells. *Bioresource Technology* 2010, **101**(9)**:** 3047-3053.

48. Chu AK, Wang JS, Tsai ZY, Lee CK. A simple and cost-effective approach for fabricating pyramids on crystalline silicon wafers. *Solar Energy Materials and Solar Cells* 2009, **93**(8)**:** 1276-1280.